Investigating constrained quantum control through a kinematic-to-dynamic-variable transformation

A. Donovan and H. Rabitz*
Department of Chemistry, Princeton University, Princeton, New Jersey 08544,USA
(Received 6 March 2014; published 9 July 2014)

A search for the variables that control a quantum system's dynamics occurs over a landscape, defined as the target objective as a function of the variables. Prior studies show that upon satisfaction of three specific assumptions, the topology of the landscape is free of suboptimal traps that could prematurely halt the search for an optimal control. One key assumption is free access to all necessary control variables; however, in practice, the controls are always limited in some fashion which may result in constraint-induced traps on the landscape. This paper aims to introduce the means to systematically explore the nature of constrained controls that yield suboptimal outcomes. The procedure utilizes *kinematic* controls, which comprise a simple set of time-independent variables, and then performs a landscape topology-preserving transformation into corresponding *dynamic* controls. The equivalent landscape topology of these two formulations permits the study of a family of dynamic controls that reflect constrained control landscape behavior. In particular, constrained dynamic controls are identified as isolated points on the landscape or as suboptimal level sets. The wide range of such dynamic controls indicates the richness and complexity of constraint-induced features on the landscape.

DOI: 10.1103/PhysRevA.90.013408 PACS number(s): 32.80.Qk, 02.30.Yy, 03.65.Aa, 02.30.Zz

I. INTRODUCTION

Quantum control experiments often operate in a closed-loop manner wherein a shaped laser pulse is identified to provide high fidelity for a particular observable. Achieving such optimal control remains an important goal for fundamental reasons as well as consideration for a broad range of potential applications [1–8]. In accord with most experiments, the majority of simulations utilize fields as controls [2,9–12], while some simulations have treated the system's Hamiltonian structure (e.g., energies and/or transition dipoles) as control variables, as could arise for the engineering of qubits [13–16] or choice of molecules from a library of possibilities. In either circumstance, the dynamics of a closed system will satisfy the Schrödinger equation

$$i\hbar\frac{\partial}{\partial t}U(t,0) = H(t)U(t,0), \quad U(0,0) = \mathbb{1}, \tag{1}$$

for $t \in [0,T]$. While the Hamiltonian $H(t)$ may assume a variety of forms, many situations are well described within the dipole approximation,

$$H(t) = H_0 - \mu\varepsilon(t) \tag{2}$$

where H_0 is the field-free Hamiltonian, μ is the transition dipole, and $\varepsilon(t)$ is the applied electromagnetic field. The unitary propagator $U(t,0)$ can be formally written as

$$U(t,0) = \mathcal{T}\exp\left(-\frac{i}{\hbar}\int_0^t H(t')dt'\right) \tag{3}$$

with $\mathcal{T}$ being the time-ordering operator. The present work considers maximization of the state-to-state transition probability $P_{i\to f}$ at time T as the goal,

$$P_{i\to f} = |\langle f|U(T,0)|i\rangle|^2. \tag{4}$$

There is generally a large family of distinctly shaped fields that can produce excellent control (for a review, see [17]). This favorable outcome can be explained by considering the search for an optimal control as a traversal over the quantum control landscape [18–20], defined as the objective as a functional of the field. The state-to-state transition probability landscape has been shown to be devoid of suboptimal extrema upon satisfaction of three assumptions [18–20]: (1) the quantum system is controllable [21,22], (2) the functions comprising the matrix $\delta U(T,0)/\delta\varepsilon(t)$ are linearly independent, and (3) there are no constraints imposed on the control variables. When these three assumptions are satisfied, the only critical points on the landscape [i.e., where $\delta P_{i\to f}/\delta\varepsilon(t) = 0, \forall\, t$] correspond to controls producing either null or perfect control.

Assumption (3) is of particular concern, as all practical control resources are subject to constraints (e.g., operation with limited fluence and/or bandwidth) [23]. With this consideration in mind, quantum control simulations have been performed with limitations placed on the control variables, including spectral component [24–26] and phase [27,28] restrictions. However, a thorough understanding of the impact of constrained control resources remains to be established. So-called kinematic control variables were introduced to investigate the impact of constraining control resources [29,30]. The latter kinematic controls were the time-independent elements of a Hermitian matrix A, ensuring the unitary of $U \equiv U(T,0)$,

$$U = \exp(iA), \tag{5}$$

with the associated kinematic state-to-state transition probability

$$P_{i\to f}(A) = |\langle f|\exp(iA)|i\rangle|^2. \tag{6}$$

Kinematic control variables were used in early landscape analyses [18], and they have also been utilized in simulations to explore search complexity [31]. Constrained kinematic controls incorporating commonly encountered dynamic analogs (e.g., limited control fluence and bandwidth) were employed

*hrabitz@princeton.edu

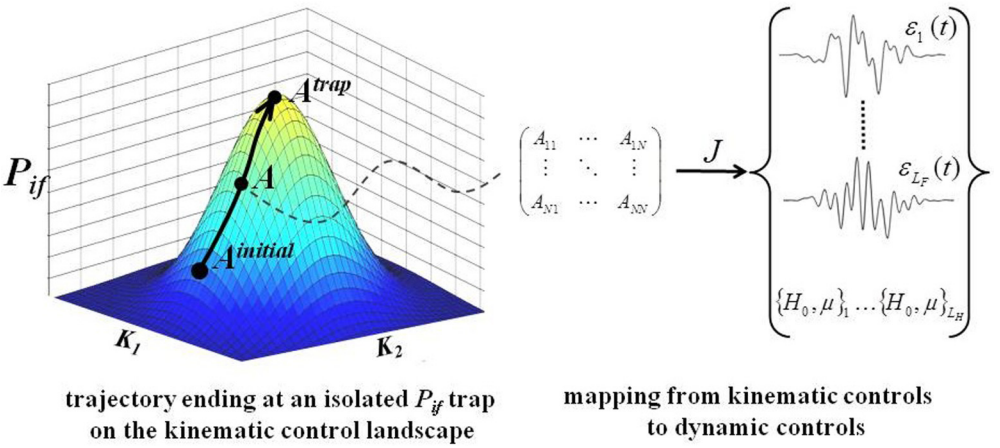

FIG. 1. (Color online) A schematic representation of the transformation from a constrained kinematic control to a family of dynamic controls. A particular kinematic control matrix A (with two controls K_1, K_2 shown, though typically a larger number of A matrix elements are admitted as control variables) obtained along a constrained state-to-state landscape ascent can be mapped to a variety of dynamic controls through the minimization of Eq. (7). Any point on the kinematic landscape, as well as the entire trajectory (represented by the bold black curve), can be transformed into a family of dynamic controls, including a number L_F of distinct fields $\varepsilon(t)$ and L_H Hamiltonian structures $\{H_0,\mu\}$.

with the aim of exploring the resulting constrained landscape's topological features [29,30]. The relatively small number of kinematic controls compared to dynamic controls (e.g., field phases or amplitudes) provides a means to view the constrained landscape in a simplified, but still physically meaningful, manner [18]. It was found that landscape traps, absent from the unconstrained landscape, can result from the use of constrained controls, and such traps can exist either as isolated points or on a level set of connected suboptimal solutions [30].

This paper aims to expand upon the prior kinematic findings and translate them into the dynamic picture through a kinematic $\rightarrow$ dynamic control transformation or mapping. The present work will provide the means to identify a diverse family of dynamic controls reflective of constrained kinematic control landscape features using the mapping procedure. At a given point on the kinematic landscape, we seek to identify a dynamic control that reproduces the kinematic results through minimization of the functional

$$J = \min_{H(t)} \|\mathcal{L}_{\rm kin}(A) - \mathcal{L}_{\rm dyn}(H(t))\|^2, \qquad (7)$$

where $\mathcal{L}$ is a metric chosen to represent what should be "conserved" upon translating between kinematic and dynamic controls, denoted collectively by $H(t)$. The two choices for $\mathcal{L}$ that will be considered in this work are the unitary matrix U and the state-to-state observable $P_{i\rightarrow f}$. Equating $\mathcal{L}_{\rm dyn}(H(t))$ to $\mathcal{L}_{\rm kin}(A)$ [e.g., full minimization of Eq. (7)], where $\mathcal{L}_{\rm kin}(A)$ is first obtained through a kinematic optimization, implies finding a dynamic control that directly reflects the kinematic control to specified precision. Figures 1 and 2 offer schematic representations of such kinematic $\rightarrow$ dynamic control transformations. Figure 1 maps a kinematic control, obtained along a $P_{i\rightarrow f}$ optimization trajectory, to two types of dynamic controls: fields $\varepsilon(t)$ and Hamiltonian structures $\{H_0,\mu\}$. Hereafter, the term "dynamic" may refer to either field or Hamiltonian structure controls, as specified, with the understanding that Hamiltonian structure controls are themselves time independent; it is also understood that some fixed reference field will be present when considering Hamiltonian structure controls. For graphical reasons, the kinematic landscape in Fig. 1 shows only two control variables K_1 and K_2, although a greater number of variables are used in practice. The indicated nonunique nature of the kinematic $\rightarrow$ dynamic control transformation can be ascribed to the generally large number of accessible dynamic control variables, permitting any number (denoted by L_F) of control

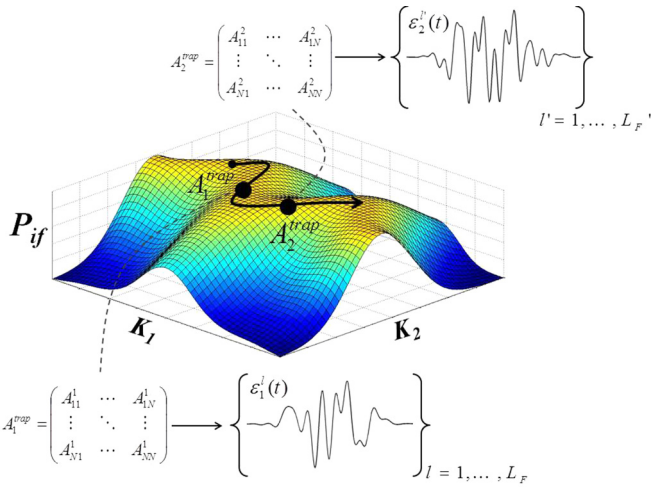

FIG. 2. (Color online) A schematic representing the transformation of trapped kinematic controls, lying on a suboptimal level set, to associated dynamic controls. Two connected kinematic control matrices $A_1^{\rm trap}$ and $A_2^{\rm trap}$ with control variables K_1, K_2 are shown that yield the same suboptimal $P_{i\rightarrow f}(A_1^{\rm trap}) = P_{i\rightarrow f}(A_2^{\rm trap}) < 1.0$. The kinematic $\rightarrow$ dynamic transformation procedure explored in the present work will show that a family of related dynamic controls can be obtained at any point along the level set to fully reflect the kinematic control topological landscape features. In this instance, $A_1^{\rm trap}$ can be mapped to a number L_F of corresponding dynamic fields $\varepsilon_1^l(t), l = 1, \ldots, L_F$; likewise, $A_2^{\rm trap}$ can be mapped to L_F' fields $\varepsilon_2^{l'}, l' = 1, \ldots, L_F'$. An analogous statement applies to a mapping to Hamiltonian structure variables $\{H_0,\mu\}$.

fields as well as L_H possible Hamiltonian structures to be identified through minimization of Eq. (7). The final point of the trajectory shown in Fig. 1, A^{trap}, represents a local isolated trap, where $P_{i\to f}(A^{\text{trap}}) < 1.0$ and any variation of the controls will result in a decreased $P_{i\to f}$ value. In contrast, the points A_1^{trap} and A_2^{trap} in Fig. 2 lie on a trap level set, where $P_{i\to f}(A_1^{\text{trap}}) = P_{i\to f}(A_2^{\text{trap}}) < 1.0$ [30]. Such trap level set topology can be favorable even for suboptimal control, as the controls possess a degree of robustness to disturbances. The generally easy to identify constrained kinematic controls and the associated landscape features can be readily transformed into dynamic controls, as indicated in Figs. 1 and 2, which motivates the framework presented here. Importantly, although there are multiple dynamic controls $H(t)$ consistent with the kinematic landscape traps, the family of dynamic controls identified in this fashion is inherently constrained to assure the same dynamic landscape topology.

The paper is organized as follows. Section II presents the constrained kinematic variable optimization algorithm and the procedure to explore the constrained kinematic landscape. Section III details the kinematic $\to$ dynamic control variable transformation. The numerical simulations in Sec. IV aim to illustrate that a variety of dynamic controls can be identified that reflect and preserve the topology of the constrained kinematic landscape. Section V provides concluding remarks.

II. MATHEMATICAL BACKGROUND

The imposition of significant constraints on control resources can introduce suboptimal traps into the nominally trap-free control landscape. This work will show that traditional dynamic controls can be identified which reflect the constrained kinematic quantum control landscape features. This section provides an overview of the mathematical tools used to (i) climb the kinematic state-to-state transition probability landscape under an imposed constraint and (ii) explore the local landscape topology at suboptimal traps. Additional details are included in the Appendices.

A. Ascending the $P_{i\to f}$ landscape with restricted control resources

The constrained optimization algorithm used in this work (a constrained implementation of the D-MORPH technique [32]) permits a systematic variation of kinematic control variables that are restricted to satisfy an imposed constraint. In this work, the controls are the M elements of a finite N-dimensional real-symmetric matrix A [cf. Eq. (5)]; the control variables can be combined into a length-M vector K,

$$K = [A_{11}, A_{12}, \ldots, A_{NN}] \tag{8}$$

where K_m denotes the mth control variable. In the present work, the maximum number of controls $M = N(N+1)/2$ is used unless otherwise noted, although they will be constrained in some fashion. The constrained optimization procedure utilizes a parameter $s \geqslant 0$ such that $K \to K(s)$ and subsequently $P_{i\to f}[K] \to P_{i\to f}[K(s)]$ in order to follow the progress of a trajectory through the control space and over the landscape. To first order, increasing $P_{i\to f}$ requires satisfying

$$\frac{dP_{i\to f}}{ds} = \nabla P_{i\to f}^{\top}\frac{dK}{ds} \geqslant 0, \tag{9}$$

where $\nabla P_{i\to f}$ is a length-M column vector containing elements $\partial P_{i\to f}/\partial K_m$, $m = 1, \ldots, M$ with [29]

$$\frac{\partial P_{i\to f}}{\partial K_m} = -2\text{Im}\Big(\langle i|U^{\dagger}|f\rangle\langle f| \int_0^1 du\, \exp[\imath(1-u)A] \times \frac{\partial A}{\partial K_m}\exp(iuA)|i\rangle\Big). \tag{10}$$

Here $\partial A/\partial K_m$ is an $N \times N$ symmetric matrix with 1 in the position(s) corresponding to the mth control variable and zeros elsewhere. We seek to determine a form for dK/ds that yields an increase in $P_{i\to f}$ while keeping an imposed constraint C fixed at an initial value C_0. A constraint considered in this work is

$$C = \|A - B\|^2 + \gamma, \tag{11}$$

where B is a real symmetric matrix and γ has a specific numerical value. Keeping $C(s) = C_0$ fixed may be viewed as forcing A to maintain a fixed γ-shifted distance from the matrix B (see Appendix B for additional commentary). While this work assumes a single constraint, multiple constraints can be treated, and the form of the constraint is flexible. The elements of B and the number γ comprise a set of L "constraint parameters" $c = [c_1, \ldots, c_L] = [B_{11}, B_{12}, \ldots, B_{NN}, \gamma]$, which are independent of s. These constraint parameters will be addressed again in Sec. II B. Satisfying the constraint $C(s) = C_0$ to first order requires

$$\frac{dC}{ds} = \nabla C^{\top}\frac{dK}{ds} = 0, \tag{12}$$

where ∇C is a length-M vector containing elements $\partial C/\partial K_m$, $m = 1, \ldots, M$. The $M \times M$ positive semidefinite projector $\mathcal{P}_{\nabla C} = [\mathbb{1} - \nabla C(\nabla C^{\top}\nabla C)^{-1}\nabla C^{\top}]$ is introduced to enable writing

$$\frac{dK}{ds} = \mathcal{P}_{\nabla C} f(s). \tag{13}$$

Setting $f(s) = \nabla P_{i\to f}$ will satisfy both Eqs. (9) and (12). By integrating the M differential equations from Eq. (13), a trajectory $K(s)$ is produced that will evolve over s until $dP_{i\to f}/ds = 0$, which may correspond to a suboptimal critical point due to the imposition of C.

B. Local trap topology

Elucidating the local topology at a constraint-induced $P_{i\to f}$ critical point requires considering $d^2P_{i\to f}/ds^2$ since $dP_{i\to f}/ds = 0$ (i.e., from utilizing the landscape ascent technique in Sec. II A). The unconstrained Hessian, containing elements $\partial^2 P_{i\to f}/\partial K_m \partial K_n$ without incorporating the constraint C, does not necessarily reflect the true landscape topology at a constraint-induced critical point. In this regard, the relevant constrained Hessian can be derived (see Appendix A) to explore the local topology of traps while enforcing the presence of the constraint [30]. The resultant constrained

Hessian has the form

$$\mathcal{H} = \nabla^2 P_{i\to f} - \nabla P_{i\to f}^{\top} \nabla C (\nabla C^{\top} \nabla C)^{-1} \nabla^2 C, \tag{14}$$

where the first term $\nabla^2 P_{i\to f}$ is the unconstrained Hessian and the second term incorporates the constraint C. The eigenstructure of $\mathcal{H}$ reveals the local landscape structure at a critical point. An isolated critical point (i.e., A^{trap} in Fig. 1) yields strictly negative eigenvalues, indicating that any variation to the controls will lead to a decrease in the observable. If the Hessian is negative semidefinite, then the corresponding controls may exist on a level set (e.g., the case in Fig. 2 for $A_1^{\text{trap}}, A_2^{\text{trap}}$). The latter topological circumstance can be desirable because the "flatness" of the trap provides a degree of control robustness that can combat a change (i.e., decrease) in the observable value in the presence of noise or other unintended control variations.

The diversity of kinematic suboptimal solutions on trap level sets may be explored, permitting variations in controls while maintaining the values of both the observable and the constraint [30]. In particular, maintaining C while traversing a level set utilizes an eigenanalysis of the "projected" Hessian $\tilde{\mathcal{H}}$,

$$\tilde{\mathcal{H}} = \mathcal{P}_{\nabla C} \mathcal{H} \mathcal{P}_{\nabla C}. \tag{15}$$

Moving on a level set with a single imposed constraint C requires that $\tilde{\mathcal{H}}$ have at least two zero eigenvalues, because the projector $\mathcal{P}_{\nabla C}$ introduces a trivial zero eigenvalue. If such an eigenstructure exists, then moving on a level set can be accomplished by solving the following differential equation:

$$\frac{dK}{ds'} = \mathcal{P}_{\nabla C} \mathcal{P}_{\tilde{\mathcal{H}}} g \tag{16}$$

where s' is a progress parameter (distinct from the previously used s to distinguish a level set trajectory from an initial constrained landscape ascent), g is a function vector of length M that may be freely chosen, and

$$\mathcal{P}_{\tilde{\mathcal{H}}} = \mathbb{1} - \sum_{j=1}^{J} \tilde{v}_j \tilde{v}_j^{\top}, \tag{17}$$

where $\tilde{v}_j$ is an eigenvector of $\tilde{\mathcal{H}}$ corresponding to a nonzero eigenvalue [30]. The choice of g will dictate the particular level set trajectory.

In some cases it is possible to vary the constraint parameters [i.e., B and γ in Eq. (11)] in order to *alter the topology* reflected in the projected Hessian while keeping the controls at their trapped value; in particular, a locally isolated trap (e.g., A^{trap} in Fig. 1) may be transformed into a level set (e.g., A_1^{trap} in Fig. 2) or even into a saddle. This process can be thought of as relaxing the constraint so as to gain favorable topological behavior (i.e., control robustness in the case of a trap existing on a level set). The associated trap topology-varying algorithm is summarized in Appendix B. The identification of constraint parameters that yield nontrivial zero $\tilde{\mathcal{H}}$ eigenvalues can be attempted through minimization of the function

$$\mathcal{F} = \text{Tr}(\tilde{\mathcal{H}}^2), \tag{18}$$

where full minimization would imply that all eigenvalues of $\tilde{\mathcal{H}}$ are identically zero. It is important to note that there is no *a priori* knowledge of whether such complete minimization is possible for an arbitrary case. Section IV will present a numerical illustration where the constraint parameters B and γ from C in Eq. (11) are varied to produce a level set of trapped kinematic solutions which can then be mapped to dynamic controls using the kinematic → dynamic control transformation in Sec. III.

III. TOPOLOGY-PRESERVING KINEMATIC → DYNAMIC CONTROL MAPS

This section presents the means to transfer from kinematic to dynamic controls. Figures 1 and 2 depict kinematic → dynamic control transformations from a particular point along a constrained kinematic trajectory and from points on a trap level set, respectively. The numerical illustrations in Sec. IV, while presenting only a few of the possible transformation solutions in any particular case, illustrate the processes suggested in Figs. 1 and 2.

Mathematically, the identification of a set of dynamic controls [denoted as $H(t)$ and representing either fields $\varepsilon(t)$ or Hamiltonian structure controls $\{H_0, \mu\}$] reflecting a constrained kinematic control A occurs through minimization of Eq. (7) with a chosen metric $\mathcal{L}$. To map an entire kinematic trajectory (i.e., a landscape ascent or a level set traversal), J may be treated as a function of the progress parameter r, where

$$J(r) = \|\mathcal{L}_{\text{kin}}(A(r)) - \mathcal{L}_{\text{dyn}}(H(r,t))\|^2 \tag{19}$$

is minimized using each kinematic control $A(r) \to A(r + dr)$ found during a kinematic trajectory. The variable r is used to represent either s or s' from Secs. II A and II B, respectively. The dynamic control used as an initial guess for the minimization of $J(r)$ is chosen as the identified dynamic control from $J(r - dr)$; in this way, a smoothly varying trajectory of dynamic controls can be obtained.

The kinematic controls considered in this work comprise a finite-dimensional matrix, while field controls lie in an infinite-dimensional function space (though in practice they are appropriately discretized in a specified manner). Thus, the transfer from a (relatively) small number of kinematic controls to fields enables the identification of diverse dynamic solutions that, upon satisfaction of the three control assumptions, will reflect the topological features of the kinematic control landscape. In this work, the transformation from a matrix A to a field $\varepsilon(t)$ considers $\mathcal{L} = U$, given a chosen fixed form of H_0 and μ. Using $\mathcal{L} = U$ also preserves $P_{i\to f}$ while imposing an additional demand on the dynamic controls in that they must reproduce the entire unitary matrix. The minimization of $J(r)$ to specified precision is performed through the application of an associated D-MORPH optimization scheme described below, although other optimization routines could be used as well. The parameter u is introduced for the goal

$$\frac{dJ(r)}{du} = \int_0^T \frac{\delta J(r)}{\delta \varepsilon(r,t)} \frac{\partial \varepsilon(r,t)}{\partial u} dt \leqslant 0, \tag{20}$$

where a trajectory is performed over $u > 0$ for each value of r. The control $\varepsilon(r,t)$ is identified through optimization of Eq. (20) where we set $\partial\varepsilon(r,t)/\partial u = -\delta J(r)/\delta\varepsilon(r,t)$. The optimization proceeds over u until the chosen tolerance of $J(r)$ is satisfied. Field amplitudes, frequencies, and/or phases may be used as control variables, but the simulations in

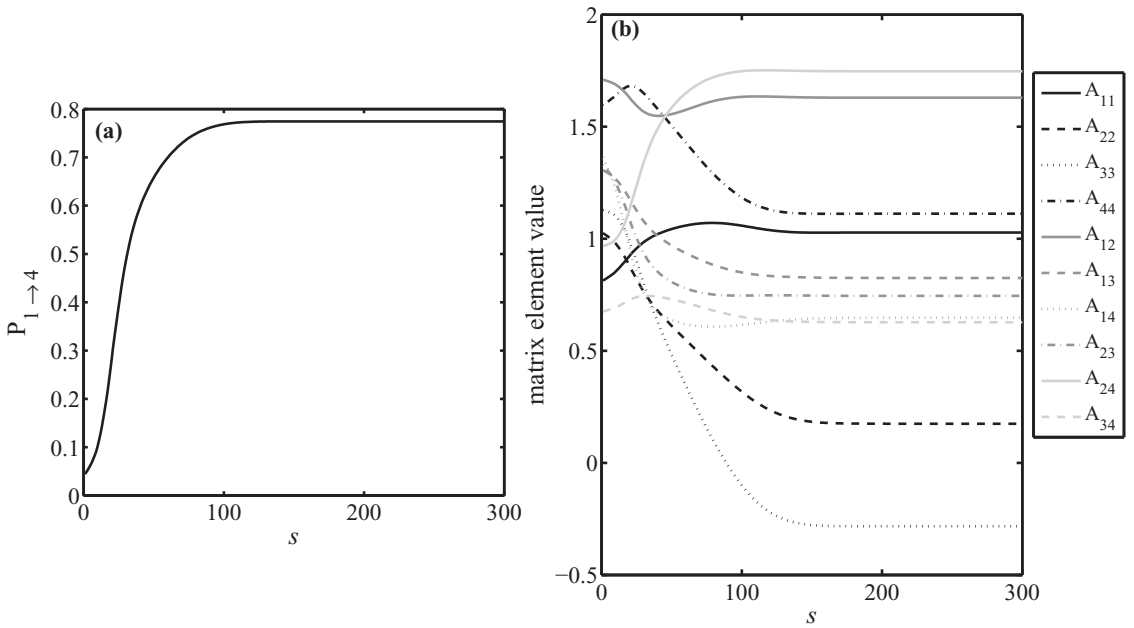

FIG. 3. Constrained kinematic optimization of $P_{1\to4}$ starting from the initial ($N = 4$)-dimensional system in Eq. (23) and terminating at Eq. (24). The constrained D-MORPH procedure introduced in Sec. II A was used to increase $P_{1\to4}$ while keeping C [cf. Eq. (11)] fixed at 4.2475 to $\sim 10^{-6}$. The final A matrix corresponds to an isolated trap at $P_{1\to4} = 0.7745$. All quantities are dimensionless.

Sec. IV will utilize the field's value $\varepsilon(t)$ at each time point as the control variables [12]. A sufficient number of time points are used for proper resolution of $\varepsilon(t)$ and for reliably solving the time-dependent Schrödinger equation [Eq. (1)]. The existence of multiple solutions for $\varepsilon(r,t)$ is evident as we may append $\partial\varepsilon(r,t)/\partial u = -[\delta J(r)/\delta\varepsilon(r,t) + h]$, with any function h orthogonal to $\delta J(t)/\delta\varepsilon(r,t)$ ensuring satisfaction of Eq. (20).

The kinematic $\to$ dynamic mapping procedure may also be used to search for time-independent elements of H_0 and/or μ [cf. Eq. (2)] from $H(t)$, again considering that assumptions (1)–(3) are satisfied. In this work, H_0 is treated as diagonal and μ assumes a real symmetric form. Kinematic controls that map to Hamiltonian structure controls are identified through minimization of

$$J(r) = \min_{H_0,\mu}[P_{i\to f}(A(r)) - P_{i\to f}(H_0(r),\mu(r),\varepsilon(\hat{t}))]^2, \quad (21)$$

i.e., $\mathcal{L} = P_{i\to f}$, where $\varepsilon(\hat{t})$ is a chosen reference field that does not vary during the search for H_0 and/or μ elements. The relevant illustrations in Sec. IV will utilize the nonlinear gradient-based optimization algorithm ("fminunc") from the MATLAB software [33] to minimize Eq. (21) over the elements of H_0 and/or μ.

IV. NUMERICAL ILLUSTRATIONS

The numerical simulations aim to illustrate the capability of identifying dynamic controls through the kinematic $\to$ dynamic mapping procedure introduced in Sec. III. This section is structured as follows. First, the constrained kinematic state-to-state transition probability is optimized. The transition $1 \to N$ is used with the understanding that this is likely demanding to maximize, particularly with the use of restricted kinematic control variables. Matrices of dimension $N = 4$ are utilized unless otherwise noted. Next, sets of fields $\varepsilon(t)$ and Hamiltonian structures $\{H_0,\mu\}$ are found that reflect the constrained landscape climb. Finally, fields that exist on trap level sets are identified. All of the simulations are presented in dimensionless units.

A. Obtaining dynamic controls for a constrained kinematic landscape climb to a trap

We consider a constrained kinematic optimization where an ($N = 4$)-dimensional kinematic system is used with the goal of maximizing $P_{1\to4}$. The constraint from Eq. (11) is chosen with $\gamma = 0$ and the randomly generated matrix B,

$$B = \begin{pmatrix} 0.4727 & 1.0716 & 0.7849 & 1.4993 \\ 1.0716 & 0.8374 & 1.2714 & 1.3817 \\ 0.7849 & 1.2714 & 0.0711 & 0.2637 \\ 1.4993 & 1.3817 & 0.2637 & 0.6505 \end{pmatrix}. \quad (22)$$

Starting from the initial randomly generated kinematic control matrix A^{initial},

$$A^{\text{initial}} = \begin{pmatrix} 0.8136 & 1.7097 & 1.3062 & 1.3618 \\ 1.7097 & 1.0248 & 1.3279 & 0.9683 \\ 1.3062 & 1.3279 & 1.1277 & 0.6761 \\ 1.3618 & 0.9683 & 0.6761 & 1.5969 \end{pmatrix}, \quad (23)$$

producing $P_{1\to4} = 0.0443$, a constrained optimization was performed using the algorithm described in Sec. II A. C was maintained to $\sim 10^{-6}$ at $C = C_0 = 4.2475$ throughout the landscape ascent. Figure 3(a) shows the monotonic increase in $P_{1\to4}$ when the elements of A vary as indicated in Fig. 3(b). At $P_{1\to4} = 0.7745$, further variation of the controls can no longer

TABLE I. Referenced data from numerical illustrations of Sec. IV.

Section	Data
Section IV A	H_0: $E_1 = 3.6584, E_2 = 6.2330, E_3 = 10.6888, E_4 = 10.7579$. μ: $\mu_{11} = 0.8009, \mu_{22} = 0.5670, \mu_{33} = 0.0074,$ $\mu_{44} = 1.8996, \mu_{12} = 1.0898, \mu_{13} = 1.6776, \mu_{14} = 1.5304, \mu_{23} = 0.8530, \mu_{24} = 0.8925, \mu_{34} = 1.3526.$
Section IV A	H_0: $E_1 = 0.5164, E_2 = 2.8594, E_3 = 10.3628, E_4 = 11.2397, E_5 = 12.8047, E_6 = 17.5198.$
Section IV B	$B_{11} = -103.18, B_{22} = 124.55, B_{33} = 66.16, B_{44} = -85.49, B_{12} = -103.03, B_{13} = -6.71, B_{14} = 160.44,$ $B_{23} = 99.53, B_{24} = -66.87, B_{34} = -67.57, \gamma = -1.50 \times 10^5.$

improve the yield in $P_{1\to4}$, where

$$A^{\text{trap}} = \begin{pmatrix} 1.0280 & 1.6293 & 0.8250 & 0.6478 \\ 1.6293 & 0.1746 & 0.7450 & 1.7473 \\ 0.8250 & 0.7450 & -0.2830 & 0.6272 \\ 0.6478 & 1.7473 & 0.6272 & 1.1120 \end{pmatrix}. \quad (24)$$

To verify that a trap was encountered, the eigenvalues of the constrained Hessian $\mathcal{H}$ from Eq. (14) were computed. All eigenvalues were negative (not shown), indicating that the trap exists as an isolated point, as an example of the case in Fig. 1.

To illustrate a few of the (infinitely) many possible dynamic controls that reflect the constrained kinematic climb above, the kinematic → dynamic transformation algorithm in Sec. III was employed to identify dynamic fields $\varepsilon(s,t)$ using each control $A(s)$ [with its associated $U(s)$] along the landscape ascent to the trap at $P_{1\to4} = 0.7745$. The chosen reference Hamiltonian structure parameters H_0 and μ used in conjunction with the field identification are listed in row 1 of Table I, and the duration of the field was chosen to be $t \in [0,10]$. The initial "trial" field [i.e., the initial guess for minimizing $J(s=0)$] contains frequency components resonant with the energy transitions arising from H_0 in Table I. Figure 4 shows two fields, one that maps to the initial kinematic control where $P_{1\to4} = 0.0443$ (dashed curve) and one that maps to the trapped control at $P_{1\to4} = 0.7745$ (solid curve). Fields were obtained for each $A(s)$ matrix along the kinematic trajectory over s, although Fig. 4 displays only the initial and final fields for clarity of presentation. No additional constraints were imposed during the mapping procedure in generating the fields in Fig. 4. A second set of identified fields are shown in Fig. 5, where in this instance a mild constraint was enforced during optimization by setting $\partial\varepsilon(t)/\partial u = -\mathcal{S}(t)\delta J_{\varepsilon(t)}/\delta\varepsilon(t)$, where $\mathcal{S}(t) = \exp[-8\pi/T^2(t-T/2)^2]$. The imposed envelope $\mathcal{S}(t)$ did not impede the mapping process [i.e., it permitted $J(s) = 1\times10^{-6}$ for each $A(s)$] in this case, while producing fields distinct from those in Fig. 4. Figures 4 and 5 illustrate the ability of the mapping procedure to identify a variety of dynamic controls that fully reflect a constrained kinematic trajectory.

In addition to finding fields, it is possible to search for elements of H_0 and/or μ as structural controls that reflect the constrained landscape climb. Figures 6(a) and 6(b) show elements of the $(N=4)$-dimensional H_0 and μ matrices, respectively, that are identified at $P_{1\to4} = 0.0443$ and $P_{1\to4} = 0.7745$ via minimization of Eq. (21) until $J(s) = 1\times10^{-6}$. The fixed reference field [$\varepsilon(\hat{t})$ from Eq. (21)] used throughout is shown in Fig. 6(c). The Hamiltonian structure element that changes the most during the optimization is μ_{14} [i.e., index 7 on the abscissa of Fig. 6(b)], going from 0.7852 to 4.2986. This behavior reflects the system's natural tendency to manipulate the element corresponding to the most "direct" pathway to the target transition, in this case

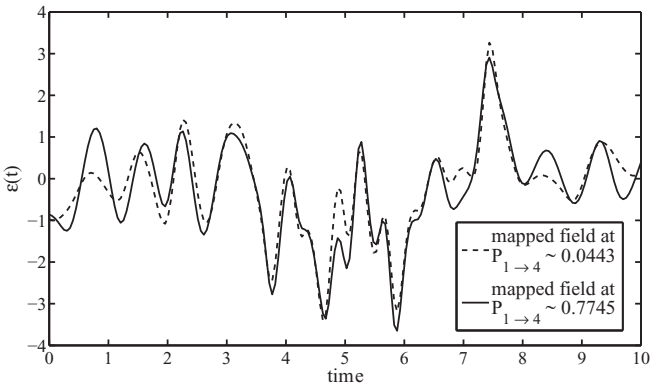

FIG. 4. Dynamic fields identified through the kinematic → dynamic control variable transformation procedure in Sec. III, corresponding to the constrained kinematic $P_{1\to4}$ landscape ascent in Fig. 3. The fields yielding the initial $P_{1\to4} = 0.0443$ (dashed curve) and final $P_{1\to4} = 0.7745$ (solid curve) are shown. No constraints were placed on the field during the mapping procedure. All quantities are dimensionless.

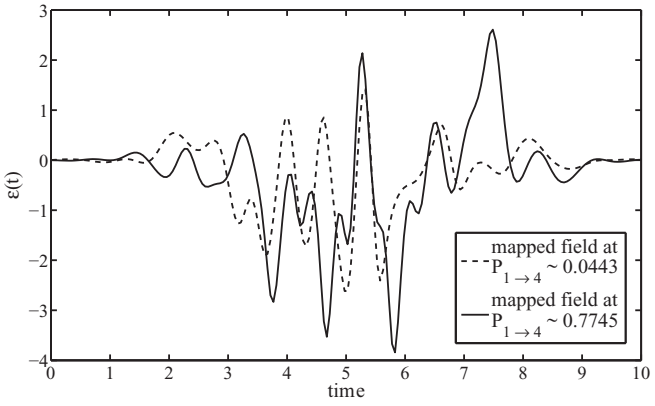

FIG. 5. Dynamic fields identified through the kinematic → dynamic control variable transformation procedure in Sec. III, corresponding to the constrained kinematic $P_{1\to4}$ landscape ascent in Fig. 3. The fields yielding the initial $P_{1\to4} = 0.0443$ (dashed curve) and final $P_{1\to4} = 0.7745$ (solid curve) are shown. During the mapping procedure, a Gaussian envelope was imposed on the fields, enforcing a structure distinct from that seen for the fields in Fig. 4. All units are dimensionless.

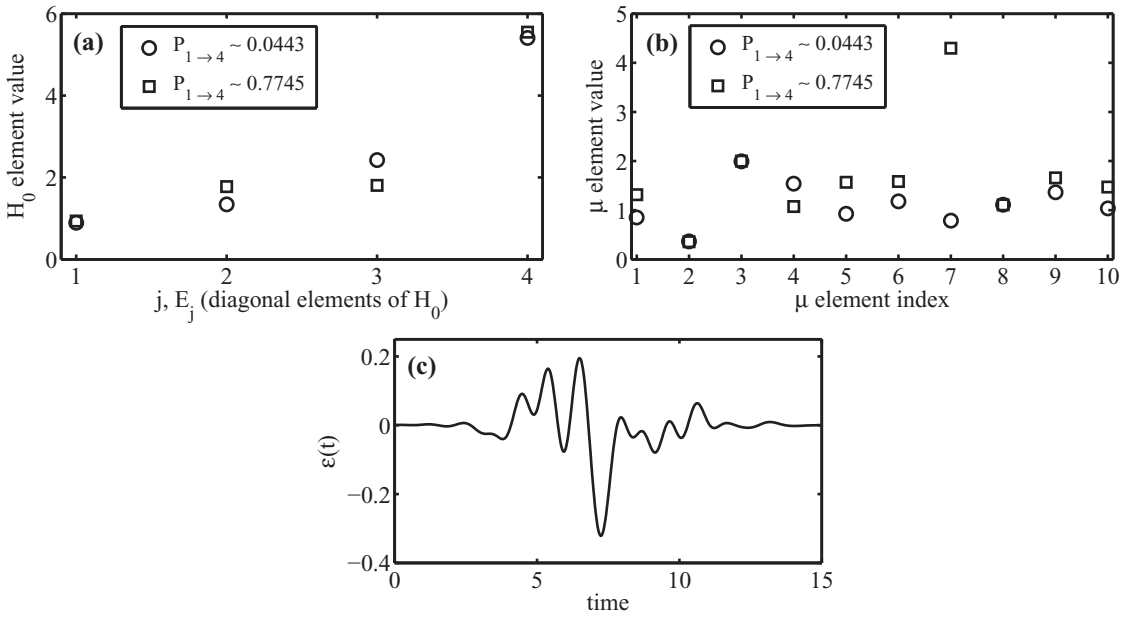

FIG. 6. (a) H_0 and (b) μ matrix elements identified through the kinematic → dynamic control variable transformation procedure in Sec. III, corresponding to the same constrained kinematic $P_{1\to4}$ landscape ascent in Fig. 3. The fixed reference field used throughout the transformation procedure is shown in (c). The matrix element μ_{14} [index 7 on the abscissa of (b)] changes most dramatically, which reflects the coupling directly to the target transition $|1\rangle \to |4\rangle$. All quantities are dimensionless.

$|1\rangle \to |4\rangle$. In mapping to Hamiltonian structure controls, changing the initial H_0 or μ elements and/or employing a different reference field can lead to the identification of distinct H_0 and μ matrix elements, giving further evidence as to the richness of the dynamic control landscape. In particular, it is possible to identify a Hamiltonian structure that utilizes multiple intermediate state transitions rather than solely manipulating the element(s) related to the direct $P_{1\to N}$ transition. As an illustration, consider an alternate kinematic constraint, specifically, a reduction in the number of admitted variables to the vector K [cf. Eq. (8)]. Using the initial ($N = 6$)-dimensional system

$$A^{\text{initial}} = \begin{pmatrix} 0.2669 & 0.2000 & 0.4492 & 0.2029 & 0.5048 & 0.4662 \\ 0.2000 & 0.0329 & 0.8219 & 0.5233 & 0.4661 & 0.5800 \\ 0.4492 & 0.8219 & 0.1283 & 0.3060 & 0.3848 & 0.7420 \\ 0.2029 & 0.5233 & 0.3060 & 0.9008 & 0.3417 & 0.8109 \\ 0.5048 & 0.4661 & 0.3848 & 0.3417 & 0.1092 & 0.6950 \\ 0.4662 & 0.5800 & 0.7420 & 0.8109 & 0.6950 & 0.2839 \end{pmatrix}, \tag{25}$$

with $P_{1\to6} = 0.0929$, a $P_{1\to6}$ optimization was performed where the following 12 elements of A were treated as fixed (i.e., they do not vary during the $P_{1\to6}$ optimization and are omitted from K): $A_{11}, A_{12}, A_{13}, A_{14}, A_{15}, A_{16}, A_{24}, A_{25}, A_{26}, A_{36}, A_{46}, A_{56}$. Figure 7(a) shows the monotonic increase in $P_{1\to6}$ as the admitted control variables (the remaining nine elements of A not listed above) change as indicated in Fig. 7(b). At $P_{1\to6} = 0.4113$, the controls [shown in bold in Eq. (26)] are no longer able to vary further and improve the yield,

$$A^{\text{trap}} = \begin{pmatrix} 0.2669 & 0.2000 & 0.4492 & 0.2029 & 0.5048 & 0.4662 \\ 0.2000 & \mathbf{1.9649} & \mathbf{-3.6413} & 0.5233 & 0.4661 & 0.5800 \\ 0.4492 & \mathbf{-3.6413} & \mathbf{-0.2348} & \mathbf{-0.0411} & \mathbf{-0.3002} & 0.7420 \\ 0.2029 & 0.5233 & \mathbf{-0.0411} & \mathbf{2.1068} & \mathbf{-3.6379} & 0.8109 \\ 0.5048 & 0.4661 & \mathbf{-0.3002} & \mathbf{-3.6379} & \mathbf{-0.1623} & 0.6950 \\ 0.4662 & 0.5800 & 0.7420 & 0.8109 & 0.6950 & \mathbf{0.0935} \end{pmatrix}. \tag{26}$$

Using these results, a search was performed to identify a dipole μ that reproduced the kinematic climb to the trap. In this case, H_0 was held fixed (values shown in row 2 of Table I). Figure 8(a) shows the changes in the μ matrix elements between the initial and final points of the kinematic landscape ascent. The elements μ_{12}, μ_{25}, and μ_{56} [with μ matrix element indices of 8, 14, and 21, respectively in Fig. 8(a)] vary the most, with μ_{16} [index 11 on the abscissa of Fig. 8(a)] only slightly changing; this circumstance implies that transitions other than $|1\rangle \to |6\rangle$ were used during the climb to the trap. Figure 8(b)

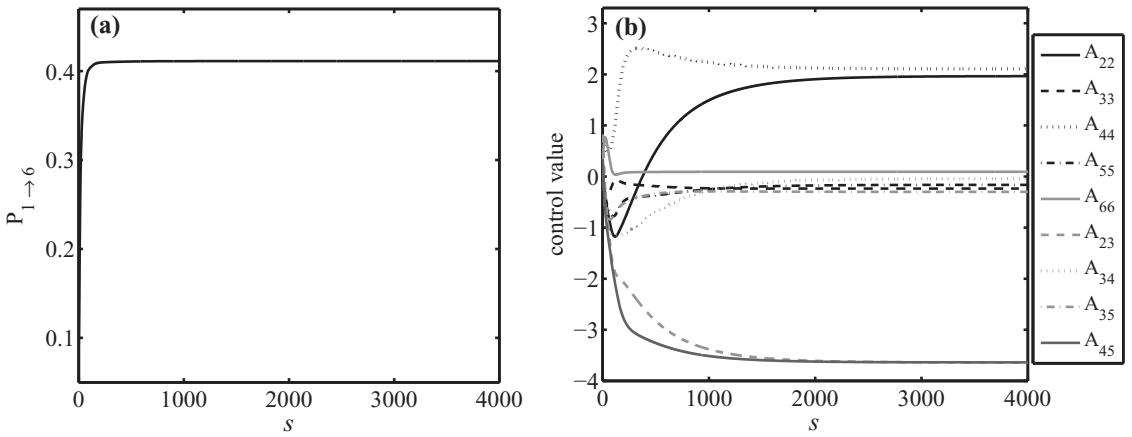

FIG. 7. (a) Increase in $P_{1\to 6}$ for an $(N = 6)$-dimensional system which is constrained by an insufficient number of control variables: 12 matrix elements of A are held fixed at randomly generated initial values [see Eq. (25)] and the remaining 9 elements are treated as control variables. The changes in the admitted controls during the landscape ascent are shown in (b). A trap is encountered at $P_{1\to 6} = 0.4113$. All quantities are dimensionless.

shows the power spectrum of the fixed reference field [$\hat{\varepsilon}(t)$ shown in Fig. 8(d)] along with the state-to-state energy transition frequencies obtained from the fixed H_0 matrix. Importantly, the frequency (17) associated with the $|1\rangle \to |6\rangle$ transition lies well outside the spectral range of the field. By contrast, the $|1\rangle \to |2\rangle$, $|2\rangle \to |5\rangle$, and $|5\rangle \to |6\rangle$ transition frequencies lie within the field's spectral range. Figure 8(c) displays the dynamic evolution of $P_{1\to j}$, $j = 1,\ldots,6$, and there is substantial contribution observed from the $|1\rangle \to |2\rangle$ transition pathway during $t \in [0,10]$ and particularly in the range $t \in [4,7]$.

B. Identifying dynamic controls along a trap level set

We now return to the original trap encountered through the imposition of C [cf. Eqs. (23) and (24) and Fig. 3]. Since the trap at $P_{1\to 4} = 0.7745$ is an isolated point, as determined from the negative definite constrained Hessian, the trapped controls

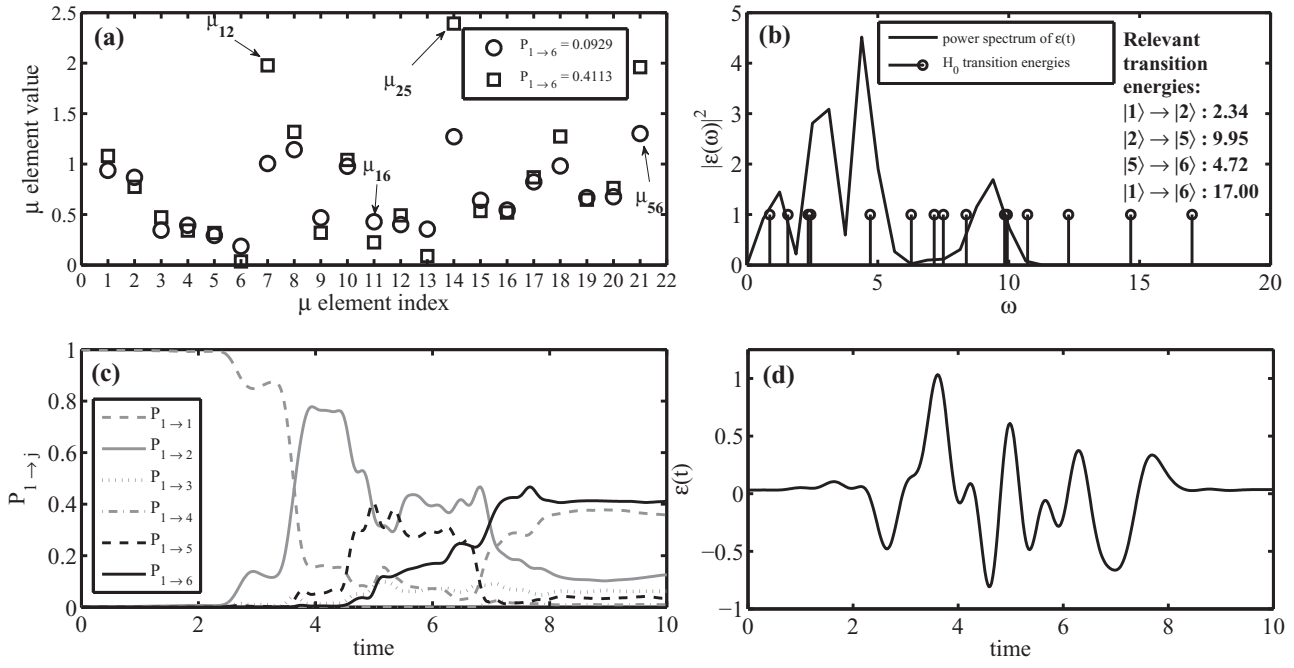

FIG. 8. Results from a search for a transition dipole matrix μ that reflects the kinematic trajectory shown in Fig. 7. (a) The initial and final values for the elements of the $(N = 6)$-dimensional μ matrix; H_0 was held fixed during the kinematic $\to$ dynamic mapping and its diagonal elements are listed in row 2 of Table I. (b) The power spectrum of the applied field [shown in (d)] with the system's natural transition frequencies arising from H_0 overlaid. Importantly, the frequency corresponding to the "direct" $|1\rangle \to |6\rangle$ transition ($\sim$17) lies well outside the spectral region of the field, while other indirect transitions show better overlap with the field's frequency components. (c) The population dynamics for all $P_{1\to j}$, $j = 1,\ldots,6$, transitions. In addition to $|1\rangle \to |6\rangle$, the $|1\rangle \to |2\rangle$ and $|1\rangle \to |5\rangle$ transitions noticeably contribute. These results indicate that various intermediate transitions, aside from the direct $|1\rangle \to |6\rangle$ transition, play important roles. All quantities are dimensionless.

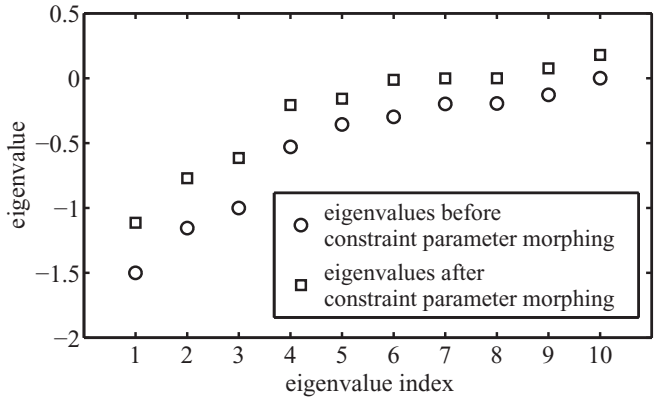

FIG. 9. Projected Hessian eigenvalues before and after the constraint parameter morphing procedure discussed in Sec. II B is performed. The constraint parameters forming C in Eq. (11) are the elements of B and the scalar γ. The eigenvalues morph from circles to squares. Importantly, the initial eigenvalues show a single zero member, which corresponds to a trivial solution arising from the imposition of the (single) constraint C. The next smallest eigenvalue is of order 10^{-1}. The constraint parameter morphing procedure was halted when an eigenvalue on the order of 10^{-3} was found. A subsequent level set traversal was then performed utilizing the newly formed projected Hessian (nontrivial) null space. All quantities are dimensionless.

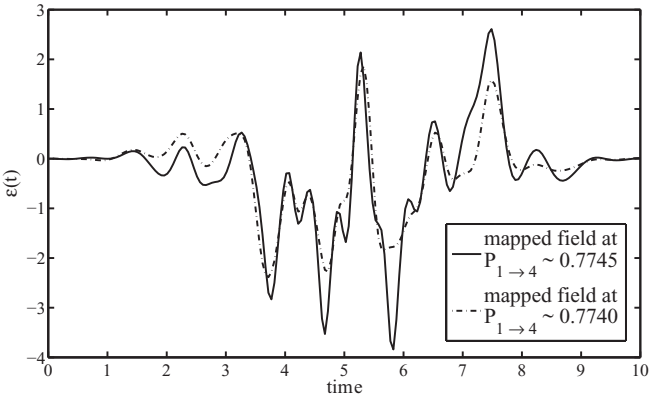

FIG. 10. Dynamic fields reflecting a kinematic trap level set traversal following the morphing of the topology of an initially isolated trap. Only the fields corresponding to the level set's initial and final kinematic controls are shown. In this instance, a Gaussian envelope was imposed on the fields during the kinematic → dynamic control transformation. All quantities are dimensionless.

do not lie on a level set. As discussed in Sec. II B, however, it is possible to attempt to create a trap level set by appropriately morphing the constraint parameters B and γ specifying the form of C, while still maintaining $C = C_0$ as a constant. In this way, a search is performed to identify a form for C that allows for the trapped controls A^{trap} to reside on a level set of suboptimal solutions; depending upon the specific case, the change in the *form* of C may be modest yet still have a significant impact. The eigenvalues of the projected Hessian [cf. Eq. (15)] were computed at the original trap and are shown in Fig. 9. The smallest nontrivial eigenvalue of $\tilde{\mathcal{H}}$ was found to be on the order of 10^{-1} (recall from Sec. II B that imposing a single constraint C leads to the generation of one "trivial" zero projected Hessian eigenvalue), which is too large to define a level set. The constraint morphing procedure was then used to vary B and γ through minimizing $\mathcal{F}$ from Eq. (18). As the minimization of $\mathcal{F}$ was performed, the eigenvalues of $\tilde{\mathcal{H}}$ were monitored, and the procedure was halted once an eigenvalue of magnitude 10^{-3} was obtained; the full set of resulting eigenvalues are shown as squares in Fig. 9. Interestingly, a saddle appears to have been identified, as indicated by the two positive eigenvalues in Fig. 9 [i.e., the minimization of Eq. (18) does not expressly prohibit positive eigenvalues from being generated]. While it is possible to continue the minimization of $\mathcal{F}$ to find even smaller eigenvalues, care is needed to assure numerical stability such that the value $C = C_0$ is maintained. In the present case, the value of $\mathcal{F}$ decreased from 5.1740 [using B from Eq. (22) and $\gamma = 0$] to 2.3176, where the final obtained B and γ are listed in the third row of Table I. The value of C was permitted to vary slightly, changing from 4.2475 to 4.2467 in order to allow for an acceptably "zero" projected Hessian eigenvalue (here, 10^{-3}).

Starting from the matrix A^{trap} in Eq. (24), a kinematic level set traversal was attempted using the new B and γ values listed in Table I by changing the controls as prescribed by Eq. (16); the free function g was a vector of randomly generated elements, and other level sets can be identified by varying the form of g (not shown). During the level set exploration, the constraint parameters now remain fixed while the elements of A are allowed to change concurrently with C and $P_{1\to4}$ being maintained at 4.2467 and 0.7745, respectively, to $\sim10^{-6}$ and $\sim10^{-4}$. The final control matrix on the level set at $P_{1\to4} = 0.7740$ is

$$A^{ls} = \begin{pmatrix} 1.4867 & 1.6249 & 0.8322 & 0.6496 \\ 1.6249 & 0.6373 & 0.7282 & 1.7412 \\ 0.8322 & 0.7282 & 0.2126 & 0.6369 \\ 0.6496 & 1.7412 & 0.6369 & 1.5721 \end{pmatrix}, \tag{27}$$

which is distinct from Eq. (24). Using the formula

$$D = \frac{\|A^{ls} - A^{\text{trap}}\|}{\sqrt{\|A^{ls}\|\,\|A^{\text{trap}}\|}} \times 100, \tag{28}$$

the percent change in A^{ls} and A^{trap} is $D = 4.6\%$. By changing the level set tolerance (i.e., varying the slight degree to which $P_{1\to4}$ is permitted to change) it is possible to obtain additional matrices showing larger variations in A matrix elements (not shown).

Given a kinematic level set trajectory (i.e., obtained in going from A^{trap} to A^{ls}), we may use the operations in Sec. III to map from kinematic to dynamic controls. Figure 10 shows dynamic fields obtained through the mapping procedure, where only the fields corresponding to A^{trap} and A^{ls} are shown for clarity of presentation. The envelope $\mathcal{S}(t)$ from Sec. IV A was imposed during the level set traversal, and the fields were identified using H_0 and μ matrices from the first row of Table I. The initial and final level set fields at $P_{1\to4} = 0.7745$ and 0.7740, respectively, show subtly distinct structural features, indicating the existence of a family of related suboptimal dynamic controls. Following Eq. (28), the percent change in the level set fields was ~25%. A trajectory of Hamiltonian

structure controls along the level set could also be obtained (not shown).

The procedure above started with a trap, morphed the form of the constraint to create a trap level set, and then locally moved on the level set to the boundary of its extent. This operation may be viewed as the first step in a continuing procedure to once again morph the form of the constraint at the boundary of the current level set seeking to expand its scope.

V. CONCLUSIONS

The growing success of quantum control in the laboratory is partly due to favorable topological features of the underlying quantum control landscape. Upon satisfaction of three key assumptions (discussed in Sec. I), the landscape lacks suboptimal traps that could prevent a local search algorithm from identifying a set of optimal control variables. In the laboratory, the assumption of access to any desired control is never fully satisfied, and the practical issue concerns operating with adequate control freedom. Significant infringement on that freedom can result in suboptimal performance. It is generally impossible to know *a priori* whether significant control restrictions are present and how they may affect performance. The present work presents a systematic means to explore the impact of control restrictions on the quantum control landscape. Specifically, this work considered the imposition of constraints on simple time-independent kinematic control variables, where significant constraints were shown to produce suboptimal traps on the landscape. Kinematic traps were encountered as isolated points as well as manifolds of suboptimal solutions. This work then developed a kinematic $\rightarrow$ dynamic variable transformation procedure to identify constrained dynamic controls (i.e., fields or Hamiltonian structure controls) that preserve the local topology of constraint-induced kinematic landscape features. The ability to identify, for example, a family of dynamic controls that reside on a trap level set provides a means to examine controls that may have desirable properties such as robustness to noise or disturbances. A forthcoming work will directly apply constraints to dynamic controls (i.e., without the use of kinematic controls) [34], and the results presented in this work indicate the complexity and richness of the constrained dynamic landscape. These collective studies aim to give insights into the trade-offs between control resources and resultant performance as a guide to considering the expansion of resources in the laboratory.

ACKNOWLEDGMENTS

The authors thank Professor Carey Rosenthal (Drexel University) for continued insight. The authors acknowledge funding from the NSF (Grant No. CHE-1058644), ARO (Grant No. W911NF-13-1-0237), ONR (Grant No. W911NF-11-1-2068), and DOE (Grant No. DE-FG02-02ER15344).

APPENDIX A: THE CONSTRAINED HESSIAN

This Appendix provides additional mathematical details regarding the derivation of the constrained Hessian $\mathcal{H}$ in Eq. (14) [29,30]. The first-order landscape ascent procedure in Sec. II A, with $f = \nabla P_{i\rightarrow f}$ in Eq. (13), leads to $dP_{i\rightarrow f}/ds = 0$ at a constraint-induced trap; from Eq. (13) and Eq. (9), this yields the trap condition $\nabla P_{i\rightarrow f}^{\top}\mathcal{P}_{\nabla C}\nabla P_{i\rightarrow f} = 0$, which implies that the gradients $\nabla P_{i\rightarrow f}$ and ∇C are parallel. Exploring the local landscape topology at the trap critical point requires consideration of $\delta^2 P_{i\rightarrow f}$, and taking a local landscape excursion at the trap demands maintaining the values of $P_{i\rightarrow f}$ and the constraint C to second order. In this regard, the following criteria must be satisfied:

$$\frac{1}{2}\left(\frac{dK}{ds'}\right)^{\top}\nabla^2 P_{i\rightarrow f}\frac{dK}{ds'}\Delta s'^2 + \frac{1}{2}\nabla P_{i\rightarrow f}^{\top}\frac{d^2K}{ds'^2}\Delta s'^2 = 0 \tag{A1}$$

and

$$\frac{1}{2}\left(\frac{dK}{ds'}\right)^{\top}\nabla^2 C\frac{dK}{ds'}\Delta s'^2 + \frac{1}{2}\nabla C^{\top}\frac{d^2K}{ds'^2}\Delta s'^2 = 0, \tag{A2}$$

where the progress parameter s' is used to distinguish the trap neighborhood excursion from the initial landscape ascent (indexed by s). After rewriting Eq. (A2) as

$$\nabla C^{\top}\frac{d^2K}{ds'^2} = -\left(\frac{dK}{ds'}\right)^{\top}\nabla^2 C\frac{dK}{ds'}, \tag{A3}$$

multiplying Eq. (A3) on the left by $\nabla P_{i\rightarrow f}^{\top}\nabla C(\nabla C^{\top}\nabla C)^{-1}$ and noting that $\nabla P_{i\rightarrow f}^{\top}\mathcal{P}_{\nabla C} = 0$ at a trap, we may write

$$\nabla P_{i\rightarrow f}^{\top}\frac{d^2K}{ds'^2} = -\nabla P_{i\rightarrow f}^{\top}\nabla C(\nabla C^{\top}\nabla C)^{-1}\left(\frac{dK}{ds'}\right)^{\top}\nabla^2 C\frac{dK}{ds'}. \tag{A4}$$

By rewriting Eq. (A1) as

$$\nabla P_{i\rightarrow f}^{\top}\frac{d^2K}{ds'^2} = -\left(\frac{dK}{ds'}\right)^{\top}\nabla^2 P_{i\rightarrow f}\frac{dK}{ds'}, \tag{A5}$$

combination of Eqs. (A4) and (A5) yields

$$\left(\frac{dK}{ds'}\right)^{\top}\left(\nabla^2 P_{i\rightarrow f} - \nabla P_{i\rightarrow f}^{\top}\nabla C(\nabla C^{\top}\nabla C)^{-1}\nabla^2 C\right)\frac{dK}{ds'} = 0. \tag{A6}$$

Thus, changing the controls K so as to keep $P_{i\rightarrow f}$ and C at their respective trapped values to second order requires that dK/ds' satisfies Eq. (A6), thereby leading to the constrained Hessian in Eq. (14).

APPENDIX B: VARYING CONSTRAINT PARAMETERS TO ALTER LOCAL LANDSCAPE TOPOLOGY

This appendix presents the means for varying the parameters specifying the form of the constraint in order to change the local landscape topology at a constraint-induced trap. In the present work, the aim is to change an isolated trap into a level set of suboptimal solutions, but the method may also be used to change the trap into a saddle [30]. In this work, the particular C in Eq. (11) contains the elements of the matrix B and the scalar γ as constraint parameters. During an initial landscape ascent, the constraint parameters and the resultant $C \equiv C_0$

are held fixed (i.e., only A changes). Upon encountering a trap, the constraint parameters can be relaxed in an effort to change the local topology in a desired manner. The following procedure permits variation of the parameters while keeping $P_{i\to f}$ and the value of $C = C_0$ fixed.

After encountering a trap, a new progress parameter u' is introduced to distinguish the changes in the controls A from those of B and γ. The constraint parameters can be combined into a length-L vector $c = [B_{11}, \ldots, B_{NN}, \gamma]$ forming $c := c(u')$. Maintaining C at its trap value upon varying c requires satisfying

$$\frac{dC}{du'} = \nabla_c C \frac{dc}{du'} = 0, \tag{B1}$$

where $\nabla_c C$ contains elements $\partial C/\partial c_l$. The projector $\mathcal{P}_{\nabla P_{i\to f}}$, written analogously to $\mathcal{P}_{\nabla C}$, can be expressed in terms of its $R = M - 1$ nonzero eigenvalues σ and corresponding eigenvectors ρ as

$$\mathcal{P}_{\nabla P_{i\to f}} = \sum_{j=1}^{R} \sigma_j \rho_j \rho_j^\top. \tag{B2}$$

Enforcing the trap condition that $\nabla P_{i\to f}$ and ∇C remain parallel implies

$$\mathcal{P}_{\nabla P_{i\to f}} \nabla C = \sum_{j=1}^{R} \sigma_j \rho_j \rho_j^\top \nabla C = 0, \tag{B3}$$

such that $\rho_j^\top \nabla C = 0$ for all j and u'; differentiating this latter term yields

$$\rho_j^\top \Lambda \frac{dc}{du'} = 0, \quad \forall\ j = 1, \ldots, R, \tag{B4}$$

where Λ is an $M \times L$ matrix with elements $\Lambda_{ml} = \partial^2 C/\partial K_m \partial c_l$. There are then $R + 1 = M$ equations that must be satisfied as c is varied over u': Eq. (B1) and the R total equations from (B4). All of these equations are of the form $p^\top dc/du' = 0$ for an associated length-L vector p, and we may define an $L \times M$ matrix Ω,

$$\Omega = \begin{pmatrix} | & & | \\ p_1 & \cdots & p_M \\ | & & | \end{pmatrix}, \tag{B5}$$

which can be used to form the $L \times L$ projector $\mathcal{P}_\Omega = \mathbb{1} - \Omega(\Omega^\top \Omega)^{-1} \Omega^\top$. This permits writing

$$\frac{dc}{du'} = \mathcal{P}_\Omega h, \tag{B6}$$

where h is a vector function that can be freely chosen to, for example, create a level set. Specifically, Eq. (18) can be differentiated as

$$\frac{d\mathcal{F}}{du'} = \left(\frac{\partial \mathcal{F}}{\partial c}\right)^\top \frac{dc}{du'} \tag{B7}$$

$$= \left(\frac{\partial \mathcal{F}}{\partial c}\right)^\top \mathcal{P}_\Omega h, \tag{B8}$$

and by setting $h = -\partial \mathcal{F}/\partial c$, F will be minimized over u'.

[1] R. Levis, G. Menkir, and H. Rabitz, Science **292**, 709 (2001).
[2] F. Grossman, L. Feng, G. Schmidt, T. Kunert, and R. Schmidt, Europhys. Lett. **60**, 201 (2002).
[3] A. Natan, U. Lev, V. S. Prabhudesai, B. D. Bruner, D. Strasser, D. Schwalm, I. Ben-Itzhak, O. Heber, D. Zajfman, and Y. Silberberg, Phys. Rev. A **86**, 043418 (2012).
[4] M. Roth, L. Guyon, J. Roslund, V. Boutou, F. Courvoisier, J.-P. Wolf, and H. Rabitz, Phys. Rev. Lett. **102**, 253001 (2009).
[5] D. Moore, H. Rabitz, S. McGrane, M. Greenfield, R. Scharff, V. Beltrani, and J. Roslund, Proc. SPIE **7304**, 730413 (2009).
[6] R. Hildner, D. Brinks, and N. van Hulst, Nat. Phys. **7**, 172 (2010).
[7] K. D. Greve, P. McMahon, D. Press, T. Ladd, D. Bisping, C. Schneider, M. Kamp, L. Worschech, S. Höfling, A. Forchel, and Y. Yamamoto, Nat. Phys. **7**, 872 (2011).
[8] J. Möhring, T. Buckup, and M. Motzkus, IEEE J. Sel. Top. Quantum Electron. **18**, 449 (2012).
[9] M. Abe, Y. Ohsuki, Y. Fujimura, Z. Lan, and W. Domcke, J. Chem. Phys. **124**, 224316 (2006).
[10] I. R. Solá, V. S. Malinovsky, and D. J. Tannor, Phys. Rev. A **60**, 3081 (1999).
[11] S. Zou, G. Balint-Kuri, and F. Manby, J. Chem. Phys. **127**, 044107 (2007).
[12] K. W. Moore, R. Chakrabarti, G. Riviello, and H. Rabitz, Phys. Rev. A **83**, 012326 (2011).
[13] S. Girvin, M. Devoret, and R. Schoelkopf, Phys. Scr. **T137**, 014012 (2009).
[14] J. Martinis, Quantum Inf. Process. **8**, 81 (2009).
[15] V. Beltrani, J. Dominy, T.-S. Ho, and H. Rabitz, J. Chem. Phys. **126**, 094105 (2007).
[16] A. Donovan, V. Beltrani, and H. Rabitz, Phys. Chem. Chem. Phys. **13**, 7348 (2011).
[17] C. Brif, R. Chakrabarti, and H. Rabitz, New J. Phys. **12**, 075008 (2010).
[18] H. Rabitz, M. Hsieh, and C. Rosenthal, Science **303**, 1998 (2004).
[19] H. Rabitz, T.-S. Ho, M. Hsieh, R. Kosut, and M. Demiralp, Phys. Rev. A **74**, 012721 (2006).
[20] T.-S. Ho and H. Rabitz, J. Photochem. Photobiol. A **180**, 226 (2006).
[21] V. Ramakrishna, M. V. Salapaka, M. Dahleh, H. Rabitz, and A. Pierce, Phys. Rev. A **51**, 960 (1995).
[22] S. G. Schirmer, H. Fu, and A. I. Solomon, Phys. Rev. A **63**, 063410 (2001).
[23] J. Roslund and H. Rabitz, Phys. Rev. A **79**, 053417 (2009).
[24] P. von den Hoff, S. Thallmair, M. Kowalewski, R. Siemering, and R. de Vivie-Riedle, Phys. Chem. Chem. Phys. **14**, 14460 (2012).
[25] M. Lapert, R. Tehini, G. Turinici, and D. Sugny, Phys. Rev. A **79**, 063411 (2009).

[26] J. Werschnik and E. Gross, J. Opt. B **7**, S300 (2005).
[27] C.-C. Shu and N. Henriksen, J. Chem. Phys. **136**, 044303 (2012).
[28] K. Moore and H. Rabitz, J. Chem. Phys. **137**, 134113 (2012).
[29] A. Donovan, V. Beltrani, and H. Rabitz, Chem. Phys. **425**, 46 (2013).
[30] A. Donovan, V. Beltrani, and H. Rabitz, J. Math. Chem. **52**, 407 (2014).
[31] K. Moore, M. Hsieh, and H. Rabitz, J. Chem. Phys. **128**, 154117 (2008).
[32] A. Rothman, T.-S. Ho, and H. Rabitz, Phys. Rev. A **73**, 053401 (2006).
[33] Computer code MATLAB, version 7.14.0.739 (R2012a) (The MathWorks Inc., Natick, MA, 2012).
[34] A. Donovan and H. Rabitz (unpublished).